NASA TECHNICAL MEMORANDUM

NASA TM X-2729

NASA TM X-2729



# TWO-DIMENSIONAL CASCADE TEST OF A HIGHLY LOADED, LOW-SOLIDITY, TANDEM AIRFOIL TURBINE ROTOR BLADE

*by John F. Kline and Roy G. Stabe*

*Lewis Research Center*
*Cleveland, Ohio 44135*

NATIONAL AERONAUTICS AND SPACE ADMINISTRATION • WASHINGTON, D. C. • MARCH 1973

| 1. Report No. NASA TM X-2729 | 2. Government Accession No. | 3. Recipient's Catalog No. |
|---|---|---|
| 4. Title and Subtitle TWO-DIMENSIONAL CASCADE TEST OF A HIGHLY LOADED, LOW-SOLIDITY, TANDEM AIRFOIL TURBINE ROTOR BLADE | | 5. Report Date March 1973<br>6. Performing Organization Code |
| 7. Author(s) John F. Kline and Roy G. Stabe | | 8. Performing Organization Report No. E-7216<br>10. Work Unit No. 501-24 |
| 9. Performing Organization Name and Address Lewis Research Center<br>National Aeronautics and Space Administration<br>Cleveland, Ohio 44135 | | 11. Contract or Grant No.<br>13. Type of Report and Period Covered Technical Memorandum |
| 12. Sponsoring Agency Name and Address National Aeronautics and Space Administration<br>Washington, D.C. 20546 | | 14. Sponsoring Agency Code |
| 15. Supplementary Notes | | |

16. Abstract

A tip region section of a low-solidity tandem airfoil blade for a turbine rotor was tested in a two-dimensional cascade tunnel at solidities of 0.736 and 0.912. Blade surface static pressures and blade exit total and static pressure and flow angle were surveyed. Blade surface velocities, wake shapes, and kinetic energy losses were analyzed and compared with values for 1.852 solidity tandem airfoil blading.



| 17. Key Words (Suggested by Author(s)) | 18. Distribution Statement |
|---|---|
| Turbine blading<br>Low solidity<br>Tandem airfoil blade | Unclassified - unlimited |

| 19. Security Classif. (of this report) | 20. Security Classif. (of this page) | 21. No. of Pages | 22. Price* |
|---|---|---|---|
| Unclassified | Unclassified | 17 | $3.00 |

* For sale by the National Technical Information Service, Springfield, Virginia 22151

Page Intentionally Left Blank

# TWO-DIMENSIONAL CASCADE TEST OF A HIGHLY LOADED, LOW-SOLIDITY, TANDEM AIRFOIL TURBINE ROTOR BLADE

by John F. Kline and Roy G. Stabe

Lewis Research Center

## SUMMARY

The 0.736 solidity tip section of a low-solidity tandem airfoil turbine blade design was tested in a two-dimensional cascade tunnel. Blade surface static pressures were measured to determine velocity distribution. Total and static pressure and flow angle in the wake were surveyed to measure losses and study flow patterns. A range of exit ideal velocities from 73 to 109 percent of design was covered. Kinetic energy losses at design exit ideal velocity were more than twice as high as those of high-solidity (1.852) tandem blading at the same conditions. Supersonic velocities, shock waves, and separation were indicated. The blades were moved closer together and opened $5.6^{o}$ to increase solidity to 0.912. Losses at design exit ideal velocity were still more than twice high-solidity losses. Separation was still indicated.

## INTRODUCTION

The NASA Lewis Research Center has been involved in a comprehensive program to study advanced turbine blade concepts directed at increasing blade loading beyond conventional values while maintaining high levels of efficiency. Two concepts that achieved promising results were tandem airfoil blading and jet-flap blading.

The first test of the tandem airfoil blade on a turbine rotor was at a mean-section axial solidity (ratio of axial chord to pitch) of 1.852 (76 blades). The total efficiency of this turbine was 89.4 percent (ref. 1). The mean section was tested in a two-dimensional cascade (ref. 2). Subsequently, a second tandem airfoil bladed turbine rotor was designed for the same overall requirements, but with the mean-section solidity decreased to 1.092 (50 blades), which is a reduction in solidity of 41 percent. The corresponding decrease in tip solidity (54 percent) was higher because of the rotor blade taper of the second turbine. Unfortunately, the performance of the second turbine de-

teriorated considerably. Total efficiency was only 86.4 percent at design speed and pressure ratio (ref. 3). Annular surveys at the rotor exit indicated that this 3-point drop in efficiency was due to poor tip region performance, with probable flow separation off the suction surface of the aft airfoil.

In view of the poor tip region performance, a cascade of blades with profiles the same as a tip region section of this low-solidity rotor was tested in a two-dimensional cascade at the Lewis Research Center. The axial solidity of this cascade was 0.736. Blade surface static pressures and blade exit surveys of total pressure, static pressure, and flow angle were taken over a range of blade exit ideal velocities to study the exit flow patterns and to calculate blade row efficiency.

A higher solidity (60 blade) configuration using the same blades set closer together on the same rotor and opened $5.6^{\circ}$ to maintain reaction is being considered for rotor tests. The 0.912 solidity "tip" section was tested in a two-dimensional cascade at the Lewis Research Center.

Results for the two low-solidity (0.736 and 0.912) cascades were analyzed and compared with results for the 1.852 solidity cascade.

## SYMBOLS

$c_a$ blade axial chord, cm

$\bar{e}$ kinetic energy loss coefficient, $1 - \left(V_m^2/V_{m,id}^2\right)$

p absolute pressure

s blade spacing along pitch line, cm

W gas velocity relative to blade on rotor

x blade surface coordinate parallel to line between leading edge circle center of forward airfoil and trailing edge circle center of aft airfoil in.

y blade surface coordinate perpendicular to x, in.

$\beta$ gas flow angle relative to blade on rotor, deg from axial

$\theta$ angle between x-coordinate and turbine rotor axis, deg

Subscripts:

b blade surface

cr flow conditions at Mach 1

id ideal of isentropic process

m station at blade exit where mixing is complete and flow conditions are uniform

max maximum

1 station at blade inlet

Superscript:

'' total state condition relative to blade on rotor

## APPARATUS AND PROCEDURE

### Blades and Cascade Tunnel

The shape and relative positioning of the airfoils of the low-solidity (50-blade) rotor blading of reference 3 are illustrated by a photograph of the three-dimensional blade mounted on the test rotor (fig. 1). In the design procedure for this blading, a tip boundary layer was incorporated into the design velocity diagrams. The resulting radial variation of rotor inlet flow angle in the boundary layer could not be accommodated in the blade design because of manufacturing limitations on blade twist. The 37.3-centimeter-radius section (0.8 cm in from the tip) is clear of these boundary-layer effects and will be used in this investigation. This section will hereinafter be referred to as the "tip" section.

Blade surface coordinates at this tip section are presented in table I. Straight airfoils were shaped and positioned as specified by these coordinates to form a full-scale cascade of six blades with an axial solidity of 0.736. The geometry of this cascade is shown in figure 2.

For the increased solidity (60-blade) configuration cascade the blades were moved closer together to a pitch of 3.909 centimeters and rotated open $5.6^{\circ}$, which increased the axial chord to 3.764 centimeter and the solidity to 0.912.

A cascade of six blades was tested in the 10.16-centimeter-span suckdown tunnel shown in figure 3. The tunnel inlet floor and ceiling were set at the design angle ($27.78^{\circ}$ from axial). The trailing edge of the ceiling was set at the stagnation point of the forward airfoil of the upper blade. The trailing edge of the floor was set below the forward airfoil and forward of the leading edge of the aft airfoil of the lower blade. The walls at the tunnel exit are approximately 7 centimeters outside the flow and roughly parallel to the design exit flow angle. In this position, the walls do not contribute substantially to the turning of the flow. The boundary layer on each sidewall was sucked away through a slot located 1.27 centimeters upstream from the blades. The aspect ratio of the 0.736 solidity cascade in this tunnel is 2.17 (span, 10.16 cm; pitch, 4.69 cm).

To determine if measurements taken at midspan of the center channel are representative, flow conditions were surveyed over a large portion of the cascade. Inlet and exit static pressures at both walls were sensed in the three center channels. Exit total and static pressure and flow angle were surveyed over the center 7.62 centimeters of span and across all channels at midspan. These measurements indicated that flow conditions were relatively uniform over the center 7.62 centimeters of the three center channels.

## Instrumentation

Surface static-pressure taps were installed at midspan on the facing surfaces of the two center blades of the cascade and on both tunnel sidewalls at the channel inlet (fig. 2). The pressure sensed by these 0.38-millimeter-diameter taps was measured with mercury manometers and recorded by photographing the manometer banks.

Flow conditions 10.2 millimeters axially downstream of the blade exit were surveyed with the rake shown in figure 4. Total pressure was sensed with a square-end 0.51-millimeter-diameter tube, static pressure with a $15^{\circ}$ wedge probe, and flow angle with a two-tube $45^{\circ}$ scarf probe. Flow conditions 1.78 millimeters axially downstream of the blade exit were surveyed with a similar rake with a shorter ($40^{\circ}$) wedge. Each rake was calibrated over the range of flow angles and velocities encountered in the test. The position of the rake is indicated in figure 2. The rake was set at midspan at the expected average flow angle; the angle was not changed during the survey. The rake was traversed parallel to the plane of the blade trailing edges at a speed of about 2.54 centimeters per minute. The pressures sensed by the three probes were measured with strain-gage pressure transducers and recorded, along with traverse position, five times per second.

Cascade inlet air temperature was measured with a thermocouple.

## Procedure

Each cascade was tested at several settings of exit ideal critical velocity ratio $\left(W/W_{cr}\right)_{m,id}$ between 0.63 and 0.94. At each setting, blade surface static pressures were recorded, wake shape surveys were made very close (1.8 mm) to the blade exit, and loss surveys were made 10.2 millimeters downstream of the blade exit.

## Data Reduction

Exit survey readings were corrected as indicated by the rake calibration and plotted against traverse distance. Mass flow, axial and tangential momentum, and static pressure bits calculated from each set of readings were integrated across the center channel for a distance of one blade pitch. Assuming constant tangential momentum, the flow continuity and force-momentum relations were used to compute the flow conditions that would exist after complete mixing had occurred. These values are designated by the subscript m.

The design total-pressure loss ratio $p''_m/p''_1$ (required to compute the design ideal velocity at the blade exit) is not presented in the design report. A value of 0.9446 was implied by the design procedure and was used to obtain the value of 0.861 for design $\left(W/W_{cr}\right)_{m,id}$.

# RESULTS AND DISCUSSION

The results for the 0.736 solidity tip section of the low-solidity (50-blade) rotor of reference 3 are presented first, in terms of blade surface velocity distribution, blade exit flow patterns, and overall blade row losses. Blade exit flow patterns and overall losses of the 0.912 solidity "tip" section of the increased solidity (60-blade) rotor configuration are then presented. Finally, results for these two low-solidity cascades are analyzed and compared with results for the 1.852 solidity mean section of the high-solidity (76-blade) rotor of reference 1.

## Performance of 0.736 Solidity Blading

Blade surface velocity distribution. - The blade surface static pressures at the midspan of the facing surfaces of the two center blades were used to develop the surface velocity distributions by using the relation

$$\left(\frac{W}{W_{cr}}\right)_{b,id} = \left\{\frac{\gamma+1}{\gamma-1}\left[1-\left(\frac{p_b}{p''_1}\right)^{(\gamma-1)/\gamma}\right]\right\}^{1/2}$$

The use of this equation assumes that the flow in the free stream is isentropic. Figure 5 shows the experimentally determined blade surface velocity distribution as a function of axial chord fraction for nominal exit ideal critical velocity ratios of 0.66, 0.83, and 0.89. The shape and size of the velocity distribution envelopes of both air-

foils indicates that high loading was achieved and a desirable load distribution was approached. A general increase in suction surface velocities is indicated along the entire length of both the forward and aft airfoils as exit ideal velocity increases. This indicates an increase in loading within the passages prior to blade choking. Two differences between the forward and aft airfoil suction surface velocity distributions are of interest. The first difference is the level of velocities. It is noted that the velocities on the forward airfoil are all subsonic, whereas they are mostly supersonic on the aft foil. The second difference is the variation in suction surface velocities near the trailing edge regions of each airfoil. The diffusion variation on the forward airfoil indicates attached flow over the range of conditions tested. However, the flattening of the velocity distribution in the trailing edge region of the aft airfoil indicates possible local flow separation at the higher exit velocity levels. Such flow separation is difficult to interpret from data from static-pressure taps, but should be indicated more clearly on total-pressure wake traces made at the blade row.

Exit wake traces. - Figure 6 shows typical variations in total pressure, static pressure, and flow angle measured across the exit plane very close to the trailing edge of two adjacent blades. Pressures are shown as fractions of inlet total pressure and the angles as determined from the probe measurements in conjunction with a calibration curve. The depth and width of the total-pressure wakes both increase considerably with exit ideal velocity, particularly on the suction side of the blade. Also, the area deficit of the wakes (which is an indicator of kinetic energy losses) is much larger for the aft airfoil than for the forward airfoil. This indicates that local flow separation and high losses probably occurred from the suction side of the aft airfoils even for the lowest exit ideal velocity tested.

The large gradient in flow angle across the blade wakes negates the validity of losses based on measurements made this close to the trailing edge (ref. 4). Therefore, loss measurements were made farther downstream, where some flow mixing and tempering of the gradients had occurred.

Blade row losses. - Figure 7 shows the same type of information as shown in figure 6, but indicates the mixing effect of increasing the measuring plane distance from the trailing edge to a station farther downstream (see fig. 2). As indicated, the maximum difference in measured flow angle was about $30^{\circ}$, which is within the calibrated accuracy of the total-pressure probe used. Also, the gradients of both total- and static-pressure traces are less severe, there is a difference between static and total pressure in the trough of the wakes, and mixing of the wakes from the forward airfoils extends across the narrower of the two free-stream regions.

Downstream wake traces such as those shown in figure 7 were used to compute aftermix kinetic energy loss coefficients and flow angles. The results are shown in figure 8. The level of loss was high, and increased considerably with exit ideal velocity.

At an exit ideal velocity ratio of 0.86, which is about the design value for the turbine of reference 3, the loss is about 0.15, which is considered to be quite high. This increase in loss with exit ideal velocity substantiates the observed trends of surface velocity and wake traces of figures 5 and 6 that indicated increased flow separation.

Blade exit flow angle was within $2^{\circ}$ of the design value at design exit ideal velocity, which indicated that the desired high level of blade loading had been approached.

## Performance of 0.912 Solidity Blading

Exit wake traces. - A comparison of total and static pressure and angle traces very close to the blade trailing edges between the 0.912 solidity (60-blade rotor design) and the 0.736 solidity (50-blade rotor design) is shown in figure 9. The traces shown were made at an exit ideal velocity ratio $\left(W/W_{cr}\right)_{m,id}$ of 0.83 for both blade cascades, which is close to the design value. The additional opening of the revised blades $5.6^{\circ}$ towards axial discussed in the section APPARATUS AND PROCEDURE is approximated by the angle traces at the bottom of the figure. It does not appear from a comparison of the total-pressure traces that a large reduction in loss resulted from increasing the solidity from 0.736 to 0.912. The wakes from the aft airfoils are somewhat narrower and deeper for the higher solidity blades, and the variation in static pressure is somewhat less. The wakes from the forward airfoils are smaller for the higher solidity blade, but both are small compared to the wakes from the aft airfoils.

Blade row losses. - Loss data were taken from surveys made with the probe moved downstream. The resulting kinetic energy loss coefficients are compared to those for the 0.736 solidity blades in figure 10. The effect of increasing the solidity from 0.736 to 0.912 was a slight decrease in loss.

## Comparison and Analysis of Losses

Shown as a solid line in figure 10 are data from reference 2, which reports similar cascade results for the mean section of the 1.852 solidity tandem rotor blade of reference 1. At exit ideal velocity ratios of 0.8 and higher, the losses for both low-solidity tip sections are more than twice as high as those for the referenced 1.852 solidity blade mean section.

The major reason for the difference in losses indicated by figure 10 is felt to be the level of velocity on the suction surfaces of the three blades indicated. Both airfoils of the mean-section blade of reference 2 had all subsonic velocities. Also, both forward

airfoils of the two tip section blades of this report had all subsonic velocities with small wakes (fig. 9). However, both aft airfoils of the two tip section blades of this report had considerable supersonic velocities with corresponding flow separation and high losses.

At the lower exit ideal velocities, the losses of all three blades of figure 10 approach each other. The reason for the decrease in loss for the lower solidity blades is probably a decrease in the peak velocity along the suction surface. This is indicated by figure 11, wherein the variation of kinetic energy loss coefficient with peak velocity on the blade surface of all three blade configurations is presented. Peak velocity occurred on the suction surface of the aft blade in all instances. Losses increased steadily as peak velocity ratio increased from 0.95 to 1.24.

## CONCLUDING REMARKS

Exit surveys were made of two cascades of tandem blades corresponding to the tip sections of a single-stage tandem rotor blade turbine. High blade loading was achieved for both low-solidity tip sections tested. Peak suction surface velocities on the aft airfoils of both blades were supersonic. The losses of both low-solidity blades at design exit ideal velocity were more than twice as high as the loss of a referenced higher solidity blade with all subsonic velocities on the suction surfaces of both the forward and aft airfoils.

Flow separation and losses of both tandem blades tested were very dependent on the peak velocity level on the suction surface prior to the diffusion region near the blade trailing edge. Once the peak velocity became about sonic, local flow separation occurred with high losses. This condition became more severe as the peak velocity increased to supersonic values. If tandem blades are considered for use as a tool to control efficiently large amounts of suction surface diffusion, care should be exercised to keep the peak surface velocity subsonic.

Lewis Research Center,
National Aeronautics and Space Administration,
Cleveland, Ohio, November 13, 1972,
501-24.

# REFERENCES


1. Lueders, H. G.: Experimental Investigation of Advanced Concepts to Increase Turbine Blade Loading. VI. Performance Evaluation of Modified Tandem Rotor Blade. NASA CR-1616, 1970.

2. Nosek, Stanley M.; and Kline, John F.: Two-Dimensional Cascade Investigation of a Turbine Tandem Blade Design. NASA TM X-1836, 1969.

3. Bettner, James L.: Design and Experimental Results of A Highly Loaded, Low Solidity Tandem Rotor. NASA CR-1803, 1971.

4. Moffitt, Thomas P.; Prust, Herman W., Jr.; and Schum, Harold J.: Some Measurement Problems Encountered When Determining the Performance of Certain Turbine Stator Blades from Total Pressure Surveys. Presented at the ASME Gas Turbine Power Conference, Cleveland, Ohio, March 16-20, 1969.

TABLE I. - BLADE SURFACE COORDINATES[a] AT 37.3-CENTIMETER-TIP SECTION OF 0.736 SOLIDITY BLADE

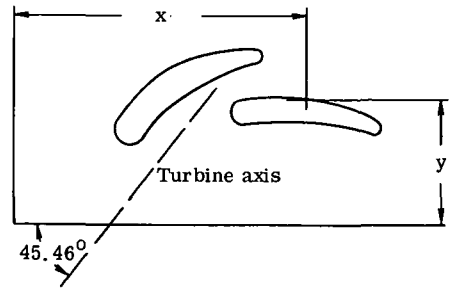


(a) Forward airfoil; leading edge circle radius, 0.0555 inch; trailing edge circle radius, 0.0150 inch

| Point | x, in. | y, in. | Point | x, in. | y, in. |
|---|---|---|---|---|---|
| 1 | 2.5486 | 3.0202 | 31 | 3.2328 | 3.4811 |
| 2 | 2.5504 | 3.0061 | 32 | 3.2232 | 3.4671 |
| 3 | 2.5456 | 3.0283 | 33 | 3.2071 | 3.4612 |
| 4 | 2.5437 | 3.0467 | 34 | 3.1910 | 3.4554 |
| 5 | 2.5429 | 3.0771 | 35 | 3.1753 | 3.4493 |
| 6 | 2.5453 | 3.1038 | 36 | 3.1517 | 3.4400 |
| 7 | 2.5508 | 3.1330 | 37 | 3.1287 | 3.4302 |
| 8 | 2.5608 | 3.1693 | 38 | 3.1061 | 3.4200 |
| 9 | 2.5733 | 3.2030 | 39 | 3.0838 | 3.4094 |
| 10 | 2.5886 | 3.2339 | 40 | 3.0620 | 3.3984 |
| 11 | 2.6061 | 3.2628 | 41 | 3.0335 | 3.3833 |
| 12 | 2.6303 | 3.2965 | 42 | 3.0056 | 3.3674 |
| 13 | 2.6567 | 3.3279 | 43 | 2.9791 | 3.3503 |
| 14 | 2.6854 | 3.3572 | 44 | 2.9534 | 3.3322 |
| 15 | 2.7223 | 3.3899 | 45 | 2.9289 | 3.3131 |
| 16 | 2.7620 | 3.4195 | 46 | 2.8997 | 3.2876 |
| 17 | 2.7979 | 3.4418 | 47 | 2.8673 | 3.2546 |
| 18 | 2.8280 | 3.4580 | 48 | 2.8368 | 3.2196 |
| 19 | 2.8598 | 3.4726 | 49 | 2.8122 | 3.1897 |
| 20 | 2.8933 | 3.4855 | 50 | 2.7886 | 3.1587 |
| 21 | 2.9291 | 3.4962 | 51 | 2.7661 | 3.1267 |
| 22 | 2.9674 | 3.5044 | 52 | 2.7485 | 3.1007 |
| 23 | 2.9976 | 3.5091 | 53 | 2.7306 | 3.0751 |
| 24 | 3.0292 | 3.5124 | 54 | 2.7122 | 3.0498 |
| 25 | 3.0620 | 3.5145 | 55 | 2.6926 | 3.0257 |
| 26 | 3.0970 | 3.5144 | 56 | 2.6771 | 3.0085 |
| 27 | 3.1351 | 3.5113 | 57 | 2.6633 | 2.9951 |
| 28 | 3.1627 | 3.5072 | 58 | 2.6515 | 2.9850 |
| 29 | 3.1914 | 3.5019 | 59 | 2.6386 | 2.9760 |
| 30 | 3.2209 | 3.4957 | 60 | 2.6282 | 2.9701 |

(b) Aft airfoil; leading edge circle radius, 0.0542 inch; trailing edge circle radius, 0.0150 inch

| Point | x, in. | y, in. | Point | x, in. | y, in. |
|---|---|---|---|---|---|
| 1 | 3.3360 | 3.0581 | 31 | 4.4577 | 3.0201 |
| 2 | 3.3375 | 3.0706 | 32 | 4.4382 | 3.0058 |
| 3 | 3.3419 | 3.0874 | 33 | 4.4157 | 3.0128 |
| 4 | 3.3470 | 3.1035 | 34 | 4.3935 | 3.0194 |
| 5 | 3.3564 | 3.1259 | 35 | 4.3653 | 3.0268 |
| 6 | 3.3723 | 3.1526 | 36 | 4.3381 | 3.0334 |
| 7 | 3.3913 | 3.1762 | 37 | 4.2984 | 3.0421 |
| 8 | 3.4125 | 3.1976 | 38 | 4.2606 | 3.0488 |
| 9 | 3.4360 | 3.2168 | 39 | 4.2238 | 3.0545 |
| 10 | 3.4619 | 3.2336 | 40 | 4.1885 | 3.0589 |
| 11 | 3.4899 | 3.2484 | 41 | 4.1425 | 3.0634 |
| 12 | 3.5201 | 3.2609 | 42 | 4.0981 | 3.0666 |
| 13 | 3.5519 | 3.2720 | 43 | 4.0543 | 3.0690 |
| 14 | 3.5937 | 3.2838 | 44 | 4.0114 | 3.0706 |
| 15 | 3.6474 | 3.2944 | 45 | 3.9691 | 3.0715 |
| 16 | 3.7049 | 3.3013 | 46 | 3.9173 | 3.0717 |
| 17 | 3.7566 | 3.3033 | 47 | 3.8563 | 3.0708 |
| 18 | 3.8008 | 3.3022 | 48 | 3.7963 | 3.0688 |
| 19 | 3.8476 | 3.2984 | 49 | 3.7470 | 3.0665 |
| 20 | 3.8981 | 3.2911 | 50 | 3.7078 | 3.0644 |
| 21 | 3.9537 | 3.2788 | 51 | 3.6688 | 3.0620 |
| 22 | 4.0158 | 3.2601 | 52 | 3.6310 | 3.0585 |
| 23 | 4.0676 | 3.2408 | 53 | 3.5943 | 3.0540 |
| 24 | 4.1245 | 3.2166 | 54 | 3.5587 | 3.0483 |
| 25 | 4.1879 | 3.1860 | 55 | 3.5248 | 3.0410 |
| 26 | 4.2557 | 3.1510 | 56 | 3.4922 | 3.0325 |
| 27 | 4.3044 | 3.1242 | 57 | 3.4606 | 3.0229 |
| 28 | 4.3573 | 3.0934 | 58 | 3.4370 | 3.0155 |
| 29 | 4.4015 | 3 0657 | 59 | 3.4213 | 3.0108 |
| 30 | 4.4531 | 3.0308 | 60 | 3.4054 | 3.0061 |

[a]These coordinates were calculated by the contractor in the design procedure for NASA CR-1804.

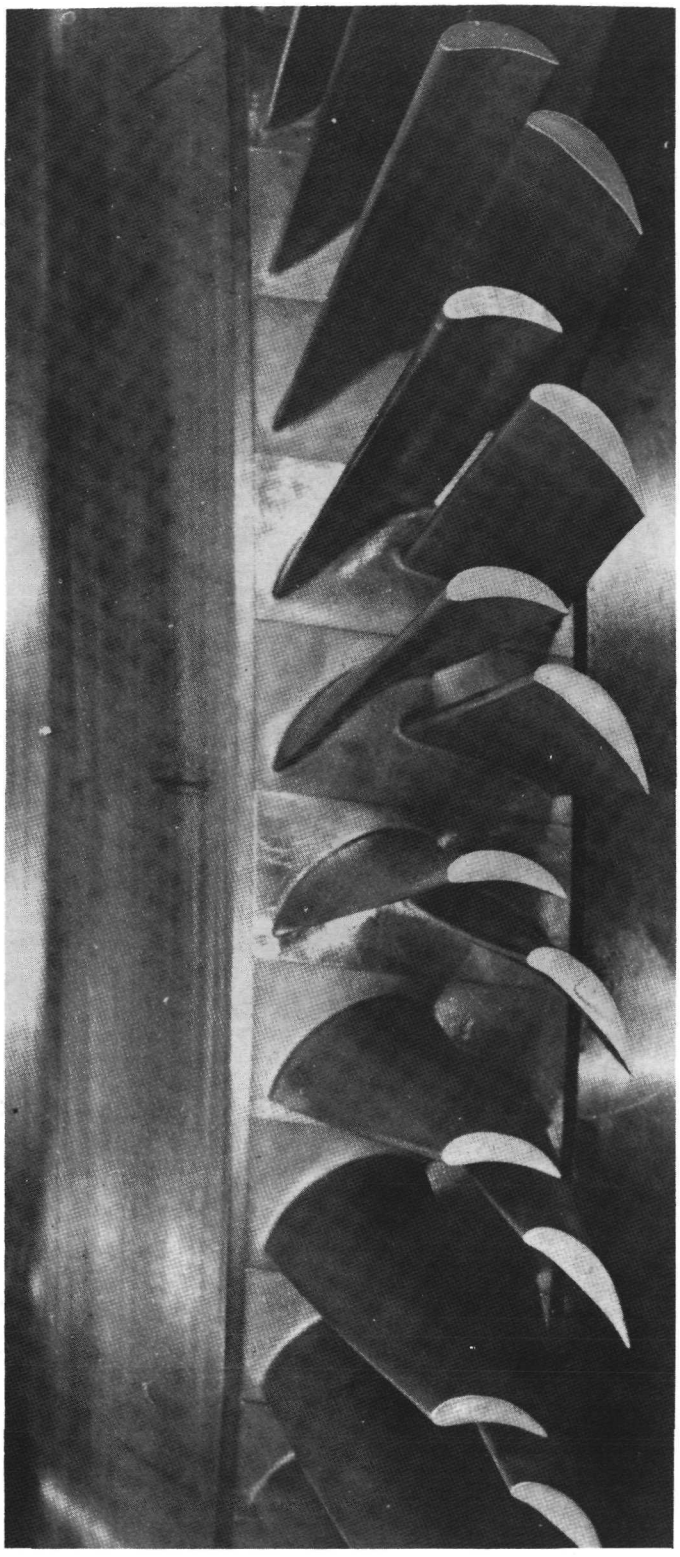

Figure 1. - Low-solidity tandem blades.

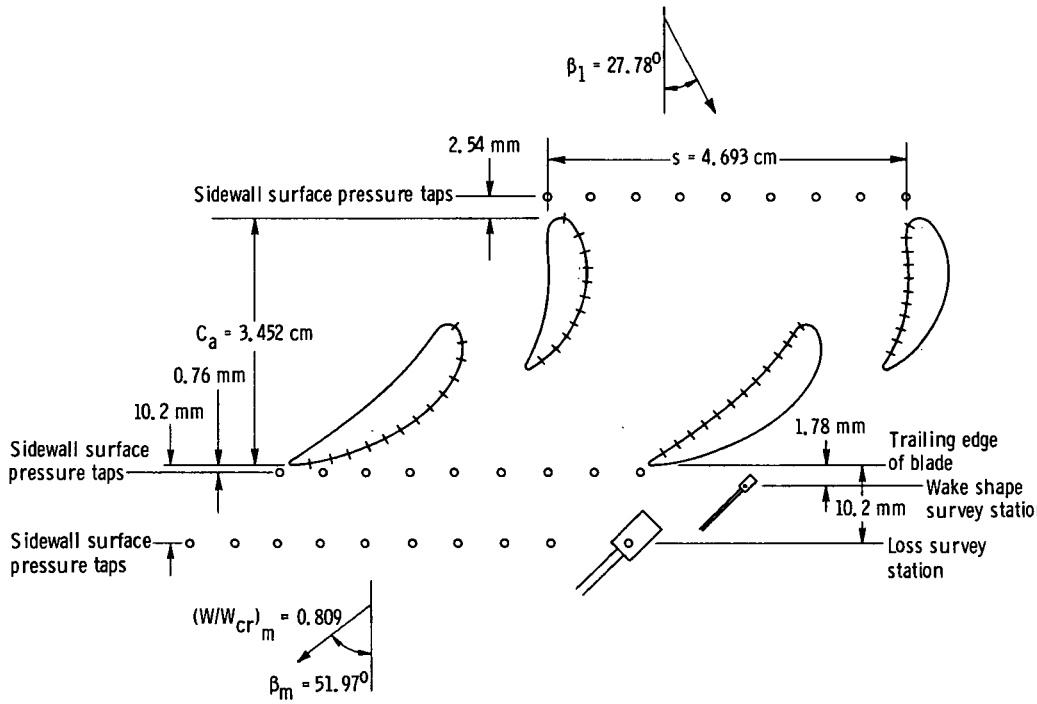


Figure 2. - Cascade geometry for 0.736 solidity blading. (Location of blade surface pressure taps indicated by hash marks.)

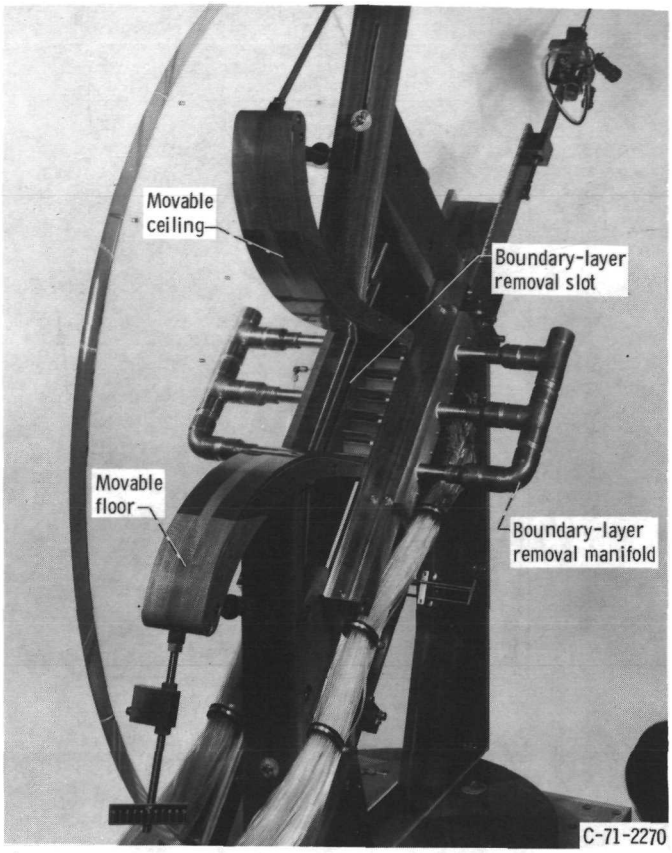


Figure 3. - Two-dimensional cascade tunnel (side removed to show details).

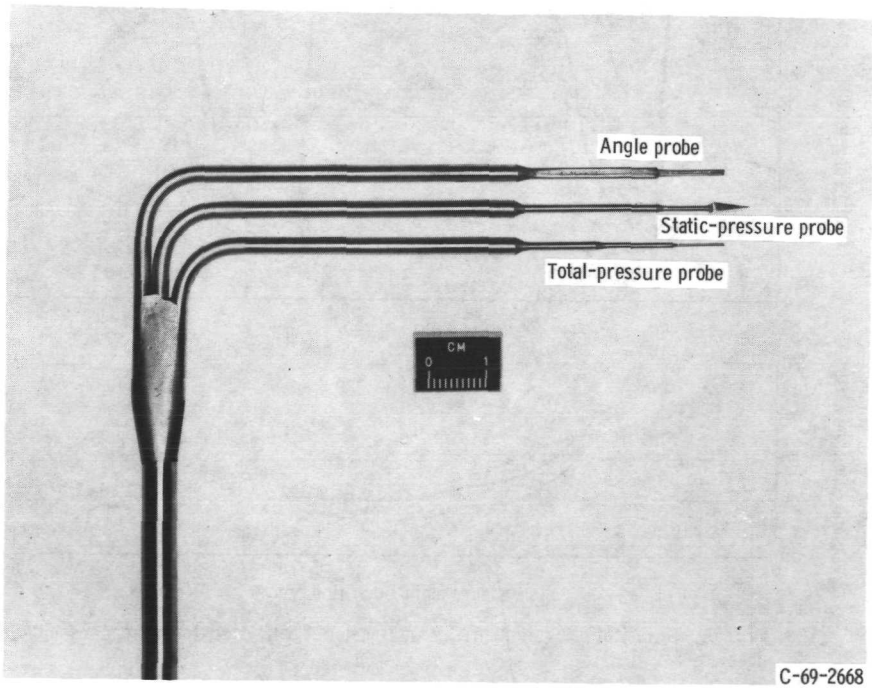


Figure 4. - Combination probe used for blade exit survey.

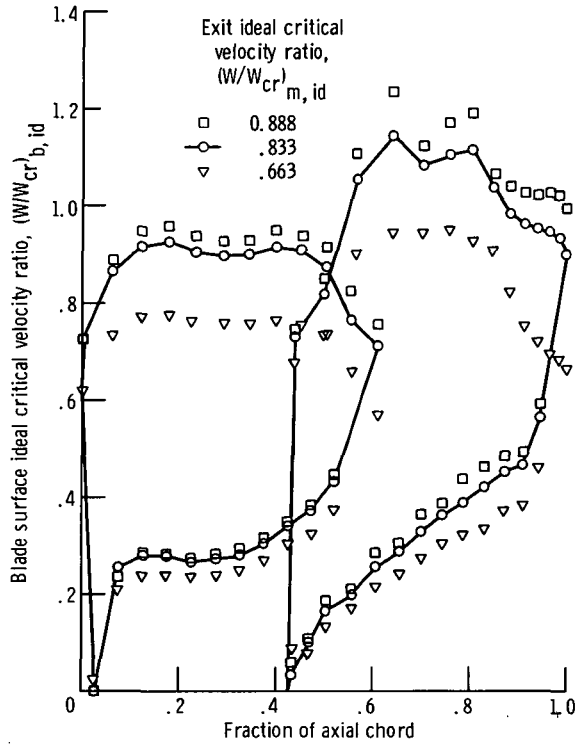


Figure 5. - Surface velocity distribution of 0.736 solidity blade.

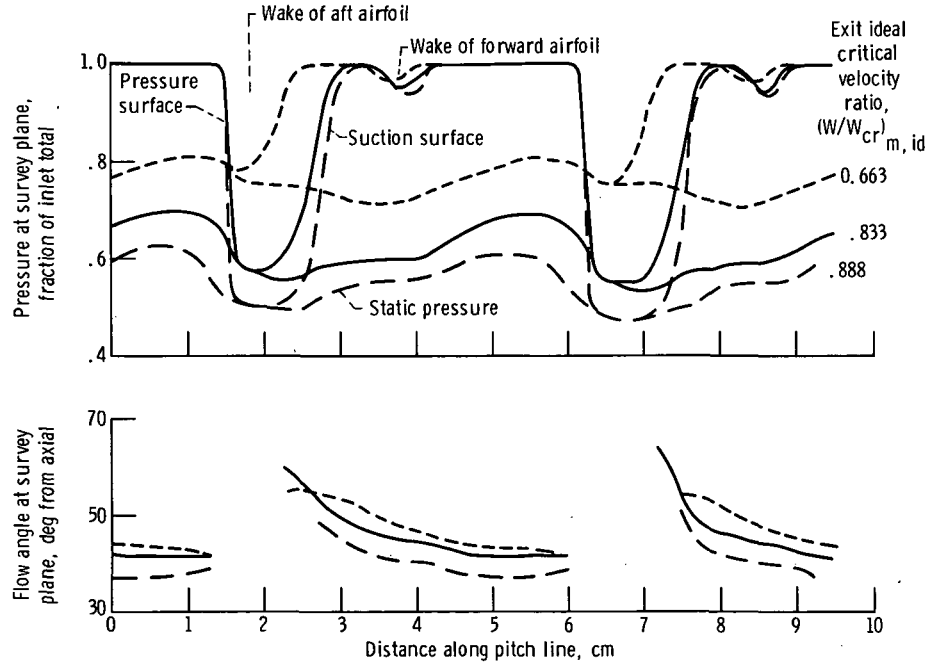


Figure 6. - Survey of flow conditions 1.78 millimeters axially downstream from exit of 0.736 solidity blade.

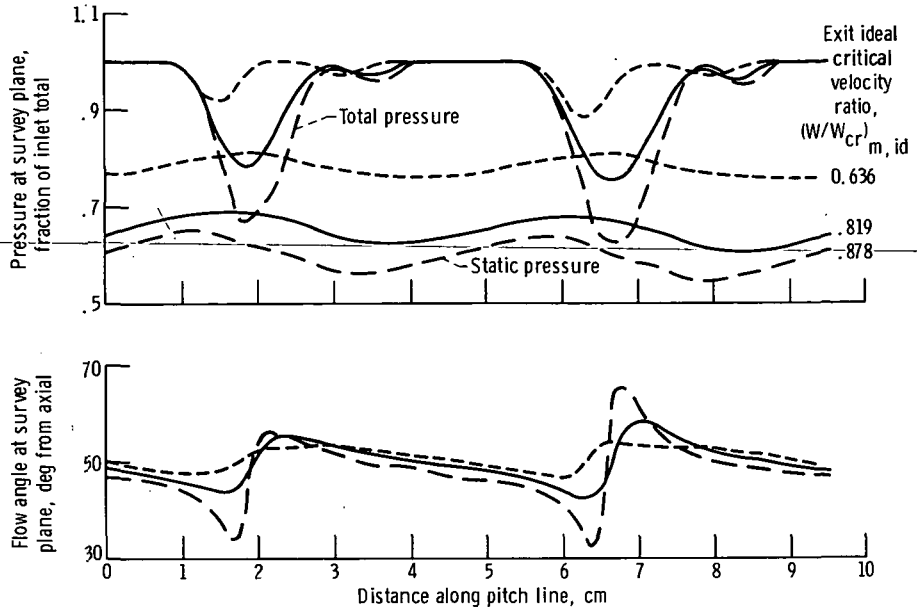


Figure 7. - Survey of flow conditions 10.2 millimeters axially downstream from exit of 0.736 solidity blade.

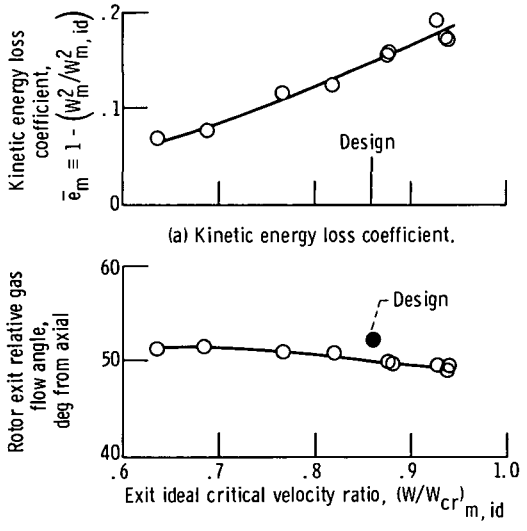


(a) Kinetic energy loss coefficient.

(b) Exit flow angle.

Figure 8. - Overall performance of 0.736 solidity blade.

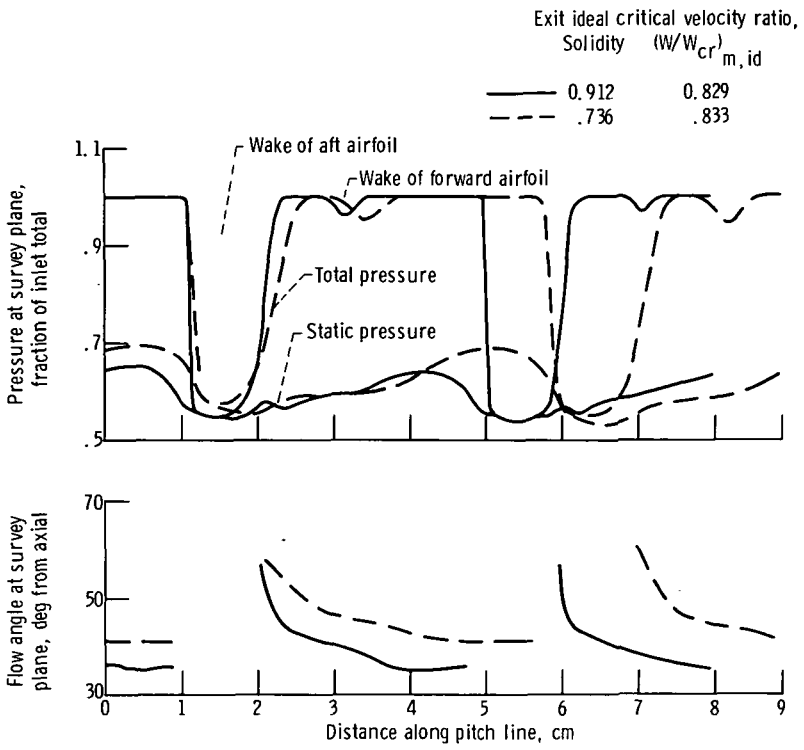


Figure 9. - Effect of solidity increase on flow conditions 1.78 millimeters axially downstream from blade exit.

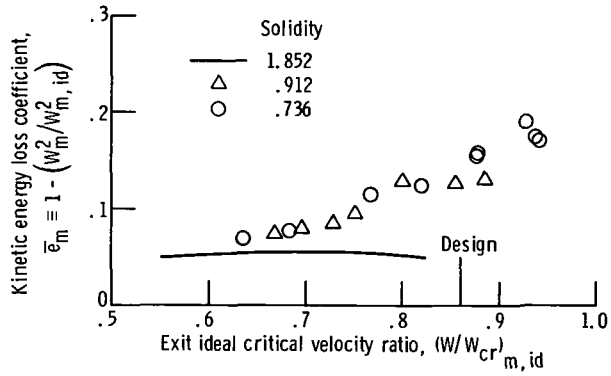


Figure 10. - Overall blade row loss comparison.

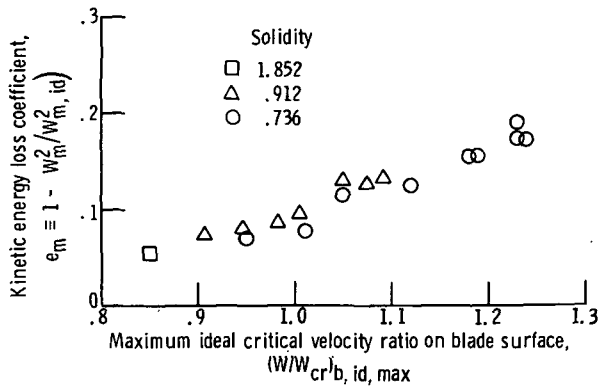


Figure 11. - Effect of blade surface maximum velocity on overall blade row loss.

NATIONAL AERONAUTICS AND SPACE ADMINISTRATION
WASHINGTON, D.C. 20546

OFFICIAL BUSINESS
PENALTY FOR PRIVATE USE $300

SPECIAL FOURTH-CLASS RATE BOOK

POSTAGE AND FEES PAID
NATIONAL AERONAUTICS AND SPACE ADMINISTRATION
451

U.S.MAIL

POSTMASTER: If Undeliverable (Section 158 Postal Manual) Do Not Return

*"The aeronautical and space activities of the United States shall be conducted so as to contribute . . . to the expansion of human knowledge of phenomena in the atmosphere and space. The Administration shall provide for the widest practicable and appropriate dissemination of information concerning its activities and the results thereof."*

—NATIONAL AERONAUTICS AND SPACE ACT OF 1958

# NASA SCIENTIFIC AND TECHNICAL PUBLICATIONS

TECHNICAL REPORTS: Scientific and technical information considered important, complete, and a lasting contribution to existing knowledge.

TECHNICAL NOTES: Information less broad in scope but nevertheless of importance as a contribution to existing knowledge.

TECHNICAL MEMORANDUMS: Information receiving limited distribution because of preliminary data, security classification, or other reasons. Also includes conference proceedings with either limited or unlimited distribution.

CONTRACTOR REPORTS: Scientific and technical information generated under a NASA contract or grant and considered an important contribution to existing knowledge.

TECHNICAL TRANSLATIONS: Information published in a foreign language considered to merit NASA distribution in English.

SPECIAL PUBLICATIONS: Information derived from or of value to NASA activities. Publications include final reports of major projects, monographs, data compilations, handbooks, sourcebooks, and special bibliographies.

TECHNOLOGY UTILIZATION PUBLICATIONS: Information on technology used by NASA that may be of particular interest in commercial and other non-aerospace applications. Publications include Tech Briefs, Technology Utilization Reports and Technology Surveys.

***Details on the availability of these publications may be obtained from:***

**SCIENTIFIC AND TECHNICAL INFORMATION OFFICE**

**NATIONAL AERONAUTICS AND SPACE ADMINISTRATION**

**Washington, D.C. 20546**